Chapter 4

A New Three-Phase AC-DC Single-Stage WECS

4.1 Introduction

Non-conventional energy sources are the only viable option to alleviate the increasing energy demand with sustainable development [106]. Compared to other renewable energy sources, wind energy is economical and more suitable for rural standalone applications [82]. In standalone WECS, a Diode Bridge Rectifier (DBR) is conventionally used for AC to DC power conversion, followed by a DC-DC converter for MPPT. The front-end DBR decreases the conversion efficiency due to conduction losses; it is reported in [67] that the elimination of the input diode bridge can increase the efficiency by around 2 percent. Thus, to increase efficiency of the WECS bridgeless AC-DC converters are optimal [39, 70–74, 107–109]. The Active Power quality improvement by eliminating the Diode Bridge Rectifier(DBR) has already been successfully achieved using a single-phase bridgeless buck [70], boost [74, 110] ćuk [72, 107–109], sepic [71, 87] converters.

In this chapter, a novel single-stage three-phase bridgeless ćuk converter is proposed. The converter is designed with the input inductors working in the discontinuous inductor current mode (DICM) while the output inductors are in continuous inductor current mode(CICM). This improves the power quality of the source side and has a low DC voltage ripple in the output [111]. A DC motor is used for emulating wind turbines, which is coupled with a self-excited induction generator(SEIG).

This chapter is organized as follows. The circuit description, operation, design, and

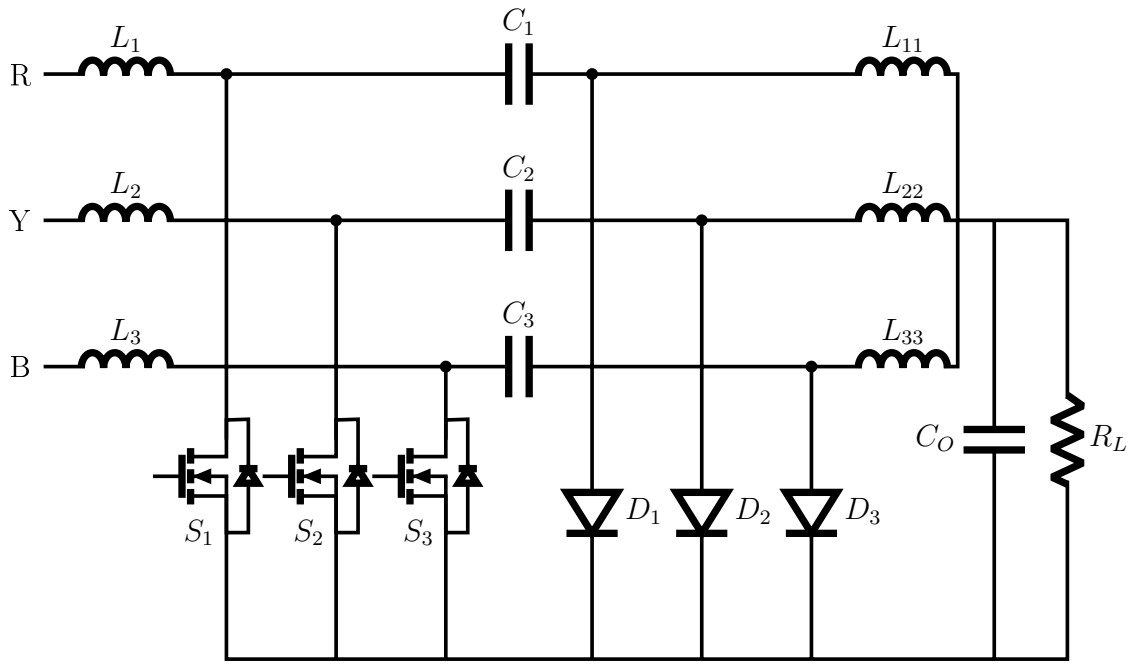

Figure 4.1: Circuit topology of the proposed converter

analysis are collated in section 4.2. The implementation technique of the wind turbine emulation is presented in section 4.3. The discussion on simulated results is done in section 4.4. Hardware results are given with a discussion in section 4.5. The conclusion regarding this work is drawn in section 4.6.

4.2 Three-Phase Bridgeless Ćuk Converter

4.2.1 Circuit description

The proposed three-phase bridgeless ćuk converter is designed to operate in a wide range of input voltage and frequency fluctuations and has the capability to maintain the desired output voltage. The wind energy is highly stochastic; thus, the wide-range voltage tracking capability of this converter makes it ideal for maximum power tracking in WECS.

The Bridgeless ćuk and sepic converters are generally used with two diodes per phase in typical configurations. In the proposed topology, the number of diodes per phase is reduced to one by using the body diodes of the MOSFETs as shown in Figure 4.1.

This converter is designed to operate at 100 kHz and discontinuous input inductor current; thus has a small inductance requirement, which leads to lower weight and size. Conventional bridgeless converters require DBR to be connected before the input

inductors. The low inductance requirement and absence of the input side DBR makes it possible to use the leakage inductance of the generator as the input inductors in the proposed converter.

4.2.2 Circuit operation

It is shown in Figure 4.1 that the input to the converter is a three-phase voltage source. The input inductors are L_1,L_2 & L_3. These input inductors are being switched by three MOSFETs namely S_1, S_2 & S_3.

As the MOSFETs are switched to 'ON' state, the input inductors start to get energized, and capacitors C_1, C_2 & C_3 begin discharging into the output capacitor C_o and load R_L through the output inductors L_{11},L_{22} & L_{33}.The operation of the proposed converter can be broadly divided into three parts as Mode-1, Mode-2 & mode-3, discussed as follows

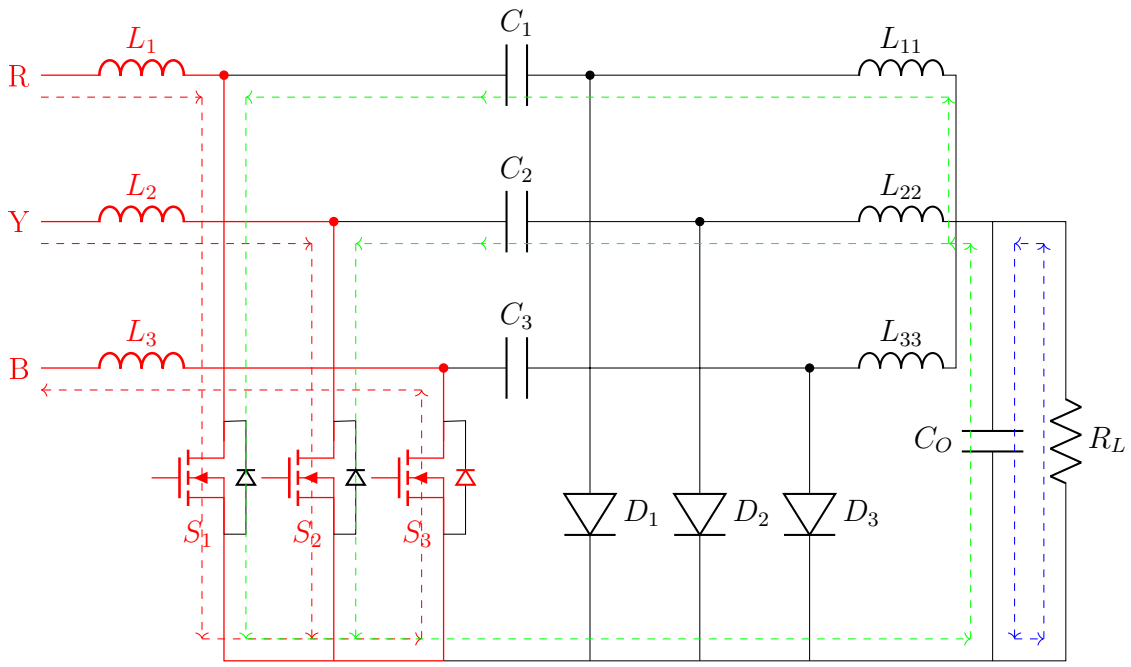

Figure 4.2: Current directions with switches in 'ON' state(Mode-1)

Mode-1

In this mode, all the MOSFETs are in 'ON' state, as shown in Figrue 4.2. The input inductors start to charge according to the applied phase voltage across them. The inductors with positive voltage start to build up a positive current, while the inductor with a

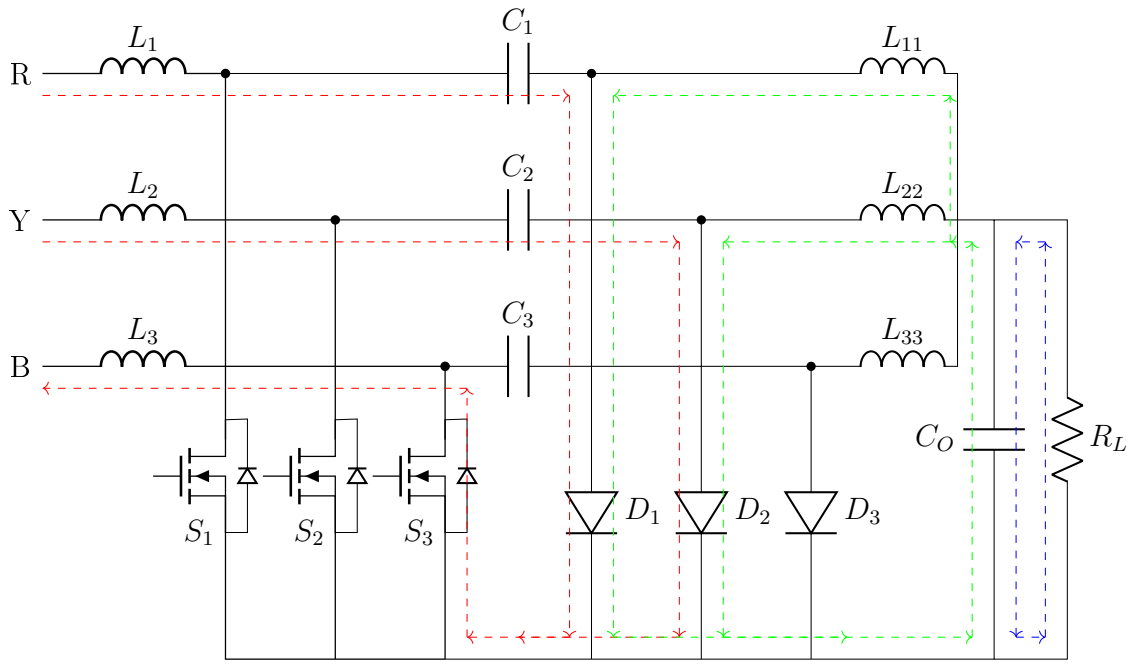

Figure 4.3: Current directions with swiches in 'OFF' state and input inductors energized (Mode-2)

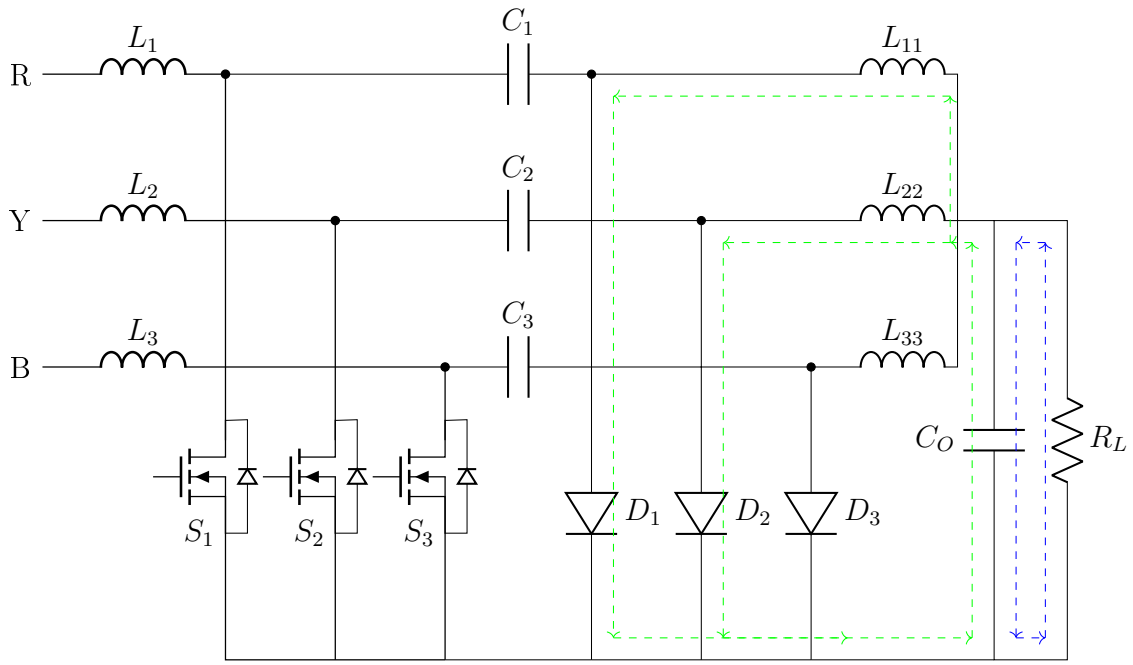

Figure 4.4: Current directions with Switches in 'OFF' state with input inductors de-energized (Mode-3)

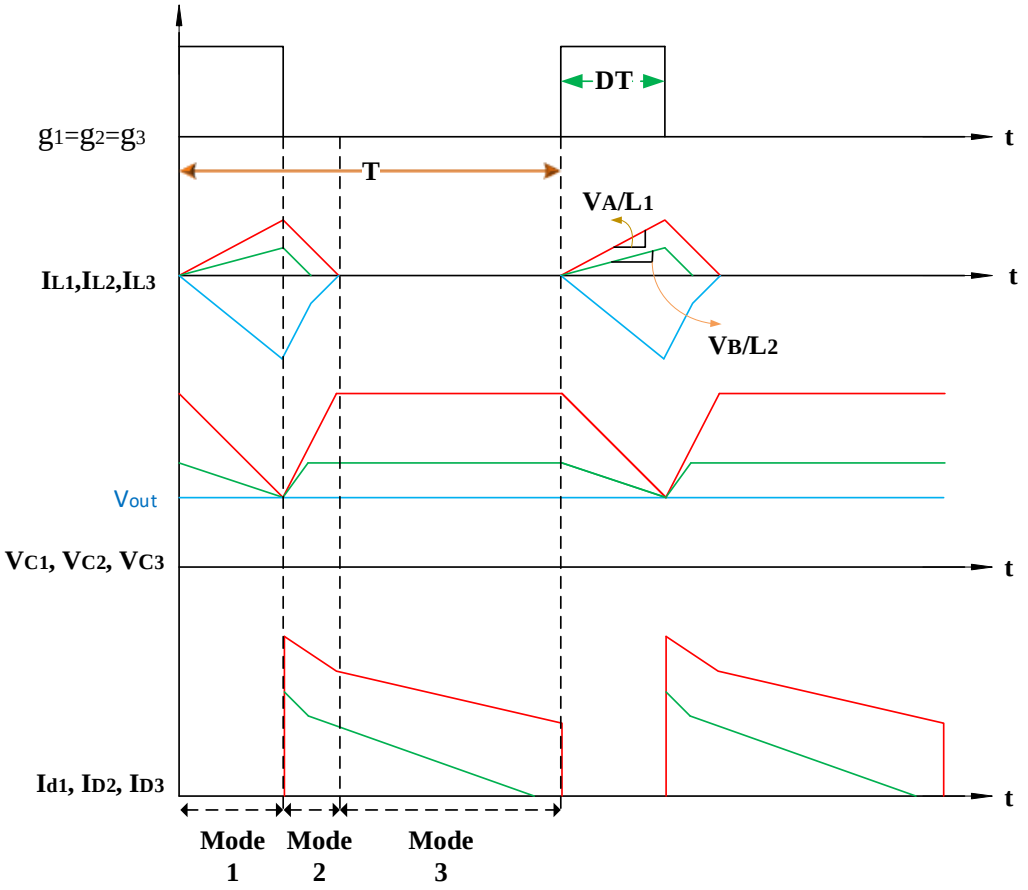

Figure 4.5: Key waveforms of the proposed converter

negative potential difference starts to build negative current across them. The capacitors having a higher voltage than the output capacitor starts to discharge through the switches and the output inductors. Figure4.4 shows the modes of operation for a particular condition in which voltages at terminal R and Y are positive, with terminal R at a higher voltage. While the terminal B is at a negative voltage.

Mode-2

In mode-2, all the switches are simultaneously switched to 'OFF' state; this marks the end of Mode-1. In this mode, the input inductors start to discharge through the capacitors C_1, C_2 & C_3 and diodes D_1, D_2 & D_3. The positive current in the input inductor/s flows through the capacitors, which increases their voltages higher than the output capacitor. The output inductor starts discharging through the diodes as the MOSFETs block the path through capacitors in the 'OFF' state. This mode carries on as long as the current

in input inductors is not zero.

Mode-3

The input inductors are fully discharged in this mode. The increased voltage across the capacitors is sustained as long as the switches are in the 'OFF' state. Only the output inductors and the diodes are in conducting state in this mode of operation. The stored energy in the output inductor is being transferred to the output capacitor. The switching of the MOSFETs to the 'ON' state marks the end of this mode.

The sinusoidally varying voltages across the three-phase supply ensure equal current sharing by the switches and diodes and thus, increase the reliability of this converter.

4.2.3 Converter design

For designing the circuit parameters, it is mathematically convenient to change the system in per phase quantity for doing the calculations as we do with three-phase electrical machines. The design parameters for the converter are given in Table 4.1. The per-phase parameters can be calculated as follow

$$\begin{aligned} Per\ phase\ voltage\ (V_{pp}) &\approx 240V \\ Maximum\ Phase\ Voltage(V_m) &\approx 340V \\ Average\ Voltage\ (V_{in}) = \frac{\sqrt{2}V_{pp}}{\pi} &= 108V \\ also\ Duty\ Cycle\ (D) = \frac{V_o}{V_o + V_{in}} &= 0.698 \end{aligned}$$

Table 4.1: DESIGN PARAMETERS

Parameter	Value
Input rms Voltage(V_{in})	415 V
Output Power(P_o)	500 W
Output Voltage(V_o)	250 V
Opearting Frequency (f)	10^5

For efficient DICM operation, the duty cycle is taken as 0.6. For Three phase system this duty becomes $0.6/3 = 0.2$.

For DICM in L_1,

Current Ripple (ΔI)=2xaverage current

$$\Delta I = \frac{2P_o}{3V_{in}} = 3.086A$$

Therefore, the inductance is calculated as:

$$L_i = \frac{V_m D T_s}{\Delta I} = 219\ \mu\text{H}$$

For Deep DICM opeartion of converter the value of input inductor is taken as 47 μH.

$$\begin{aligned}(K_a)_{critical} &= \frac{1}{2(1+M)^2} \\ &= \frac{1}{2[(V_o/V_m)+1]^2} = 0.33159\end{aligned}$$

As, $K_a < (K_a)_{critical}$

Hence, K_a is taken as 0.25. After determining K_a, the equivalent Inductance of the circuit can be calculated by using:

$$\begin{aligned}L_{eq} = \frac{R_o T_s K_a}{2} &= \frac{250^2 * 10^{-5} * 0.25}{2 * 500} \\ &= 156.25\mu\text{H}\end{aligned}$$

Hence, the value of output inductor can be calculated as:

$$L_o = \frac{L_i * L_{eq}}{L_e q - L_i} = 67\mu\text{H}$$

As the output inductor is intended to be in CICM, an inductor value of 560 μ henry is chosen in this work.

The value of the capacitor is calculated by using the filter equation. Taking the frequency at the logarithmic mean of 10^5 Hz and 50 Hz (F_s=2250 Hz), capacitance C is calculated as

$$C = \frac{1}{(2 * \pi * 2250)^2 (47 + 560) 10^{-6}} = 8.3457\mu\text{F}$$

Thus taking the amount of leakage current into account, capacitors are chosen at the commercially available value of 1 μ F. The designed parameters of the circuit are summarized in Table 4.2.

The value of the output capacitor is taken as 1000 μ F as it is high enough to bring down the voltage ripples to less than 2 percent of the output voltage at the rated load.

Table 4.2: DESIGNED CONVERTER PARAMETERS

Parameters	Value
Input Inductor (L_i)	47 μ H
capacitor (C)	1 μ F
Output Inductor (L_o)	560 μ H
Output Capacitor (C_o)	1000 μ F

4.2.4 Converter analysis

The designing was done in order to keep the input inductor in deep DICM. Thus converter analysis is also done with the same consideration. For finding the converter voltage gain V_o/V_{in}, its necessary to find the voltages across each input inductor.

$$V_R = V_m \sin(\omega t) \tag{4.1}$$

$$V_Y = V_m \sin(\omega t + 2\pi/3) \tag{4.2}$$

$$V_B = V_m \sin(\omega t - 2\pi/3) \tag{4.3}$$

On adding the squares of the above voltages we get;

$$V_R^2 + V_Y^2 + V_B^2 = \frac{3}{2} V_m^2 \tag{4.4}$$

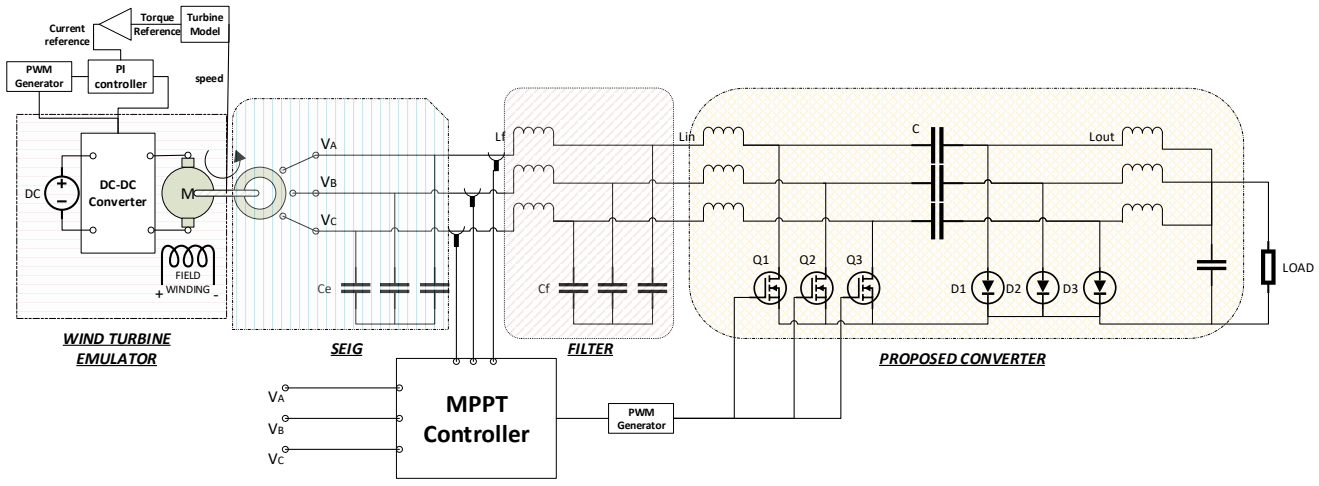

Figure 4.6: The schematic diagram of wind energy emulation and conversion system

Now, as the energy absorption is done in Mode-1 of the converter operation, the energy

absorbed in Mode-1 by input inductors in 'dt' seconds can be written as:

$$dE = Voltage * (Current\ at\ time\ t) * dt \tag{4.5}$$

$$= V_L * \frac{V_L t}{L} dt \tag{4.6}$$

Thus, total energy absorbed per phase in DT time is:

$$\Delta E = \int_0^{DT} \frac{V_L^2 t}{L} dt \tag{4.7}$$

$$= \frac{V_L^2 D^2 T^2}{2L} \tag{4.8}$$

The Total Energy absorbed can be calculated by using (4.4) & (4.8). The inductors with negative currents also discharge their energy in the capacitors. This energy is then transferred to the output capacitor. Thus the total energy can be written as:

$$\Delta E_T = \frac{D^2 T^2}{2L} * (V_R^2 + V_Y^2 + V_B^2) \tag{4.9}$$

Which can be written as:

$$= \frac{3D^2 T^2}{4L} V_m^2 \tag{4.10}$$

The (4.10) represents the total energy input to the converter in DT time. It can be noted here that the energy absorption is only happening for the DT time, as the total time cycle is of T seconds. The input power can be written as:

$$P_{in} = \frac{\Delta E_T}{T} \tag{4.11}$$

$$\implies P_{in} = \frac{3D^2 T V_m^2}{4L} \tag{4.12}$$

$$\therefore P_{out} = \eta P_{in} \tag{4.13}$$

$$\implies P_{out} = \frac{V_o^2}{R_L} \tag{4.14}$$

thus

$$V_{out} = \sqrt{\eta P_{in} R_L} \tag{4.15}$$

$$\implies V_o = \sqrt{\frac{3\eta T}{L}} \frac{D V_m}{2} \tag{4.16}$$

4.3 Wind Turbine Emulation

A separately excited DC motor is used for wind turbine emulation in this work. The armature current control method is used for generating the torque-speed characteristic of a wind turbine. In the developed system, a two-blade wind turbine(MOD2) is emulated, as these turbines have the maximum power coefficient (C_P) at around a tip speed ratio (λ) of 7. This value of λ ensures voltage generation from the mechanically coupled self-excited induction generator(SEIG).

The mechanical power output of the turbine is:

$$Pm = \frac{1}{2} C_p \rho A W^3$$

Where, C_p is a well established function of λ and pitch angle(β). An approximate model of performance coefficient for MOD 2 wind turbine is given in [112] as a non-linear function given by:

$$C_p = C_1(C_2 - C_3 v - C_4 v^x - C_5) e^{-c_6(\lambda,\theta)}. \tag{4.17}$$

where,

$$C_1 = 0.5, \qquad C_2 = 116/\lambda_i, \qquad C_3 = 0.4$$
$$C_4 = 0, \qquad C_5 = 5, \qquad C_6 = 21/\lambda_i.$$

4.3.1 MPPT and control

The availability of wind energy is stochastic in nature. This necessitates the implementation of an MPPT technique to decrease overall cost by maximizing utilization. Generally, MPPT techniques in wind systems are based on the DC link voltage and current or by measuring the blade speed and torque of the generator. With miniaturization and mass production of voltage and current sensors, they are extensively being used for condition monitoring and system control.

In this chapter, a unique MPPT technique is implemented by measuring the three-phase voltages and currents of the generator. Figure 4.7 shows a flowchart showing the MPPT technique used. As shown in (4.4), a DC value proportional to three-phase quantities can be calculated. Using these proportional DC values of voltage and current of

width=8cm[h]

Table 4.3: TURBINE PARAMETERS

PARAMETERS	VALUES
BLADE SWEEP AREA	2 m^2
Air density	1.225 kg/m^3
wind speed	8-12 m/s
Torque constant of DC motor	1.07 Nm/A
proportional constant (Kp)	0.3
integral constant (Ki)	6

the generator, the duty cycle of the AC-DC converter can be adjusted accordingly to get maximum power. The control of the emulator can be easily implemented by measuring the speed of the DC motor to generate a reference torque using (4.17). The torque applied by the DC motor is calculated by multiplying the measured armature current by the torque constant. The DC motor torque is then controlled by using a PI controller. The assumed parameters for the turbine, and values of Kp and Ki, are given in Table 4.3.

4.4 Simulation and Discussion

The simulation of the proposed converter is done in Matlab Simulink 9.0 as per the parameters given in Tables 4.2 & 4.3. The system performance on the basis of the input voltage, MPPT technique, output voltage, inductor current, and switching stress is done. It is evident from the Figures. 4.8 & 4.10 that the proposed system is working as per the design considerations.

Figure 4.9 shows the voltage and current at the input side of the filter. A lowpass LC filter is used in this circuit, with inductors of 560 mH and AC capacitors of 10 μF. As the circuit is connected with the generator at 0.7 s, current waveforms exhibis the transients as the LC filter is energized. The MPPT technique is dependent on the calculated values of voltage and current maxima. These values are shown in Figure 4.10.

The input inductor is working in deep DICM, and the calculated voltage and current maxima values are DC in nature. The output inductor is intended to work in the CICM for output DC voltage to have low ripples. Figure 4.11 shows that the output inductor

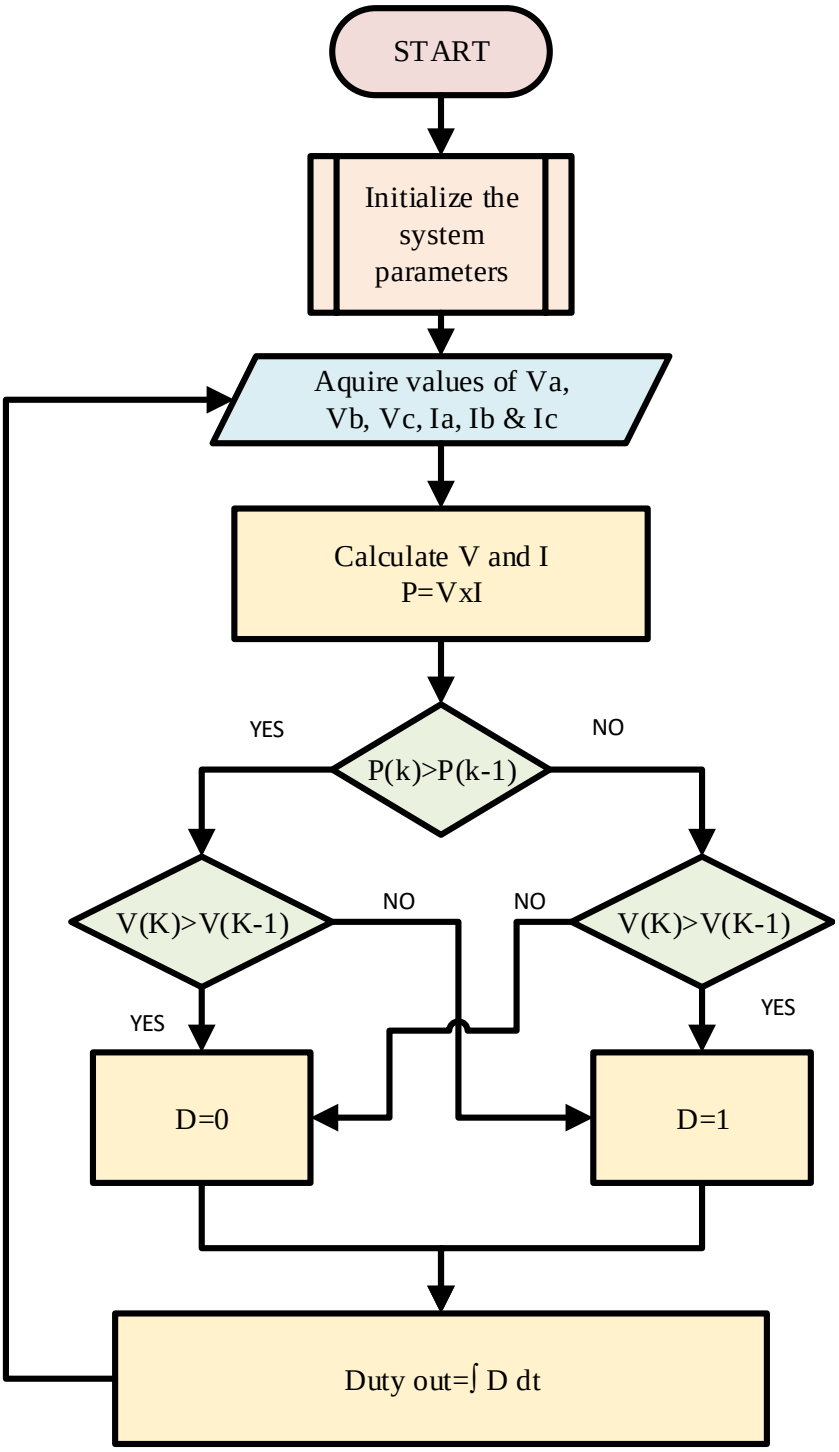

Figure 4.7: Flowchart of MPPT technique

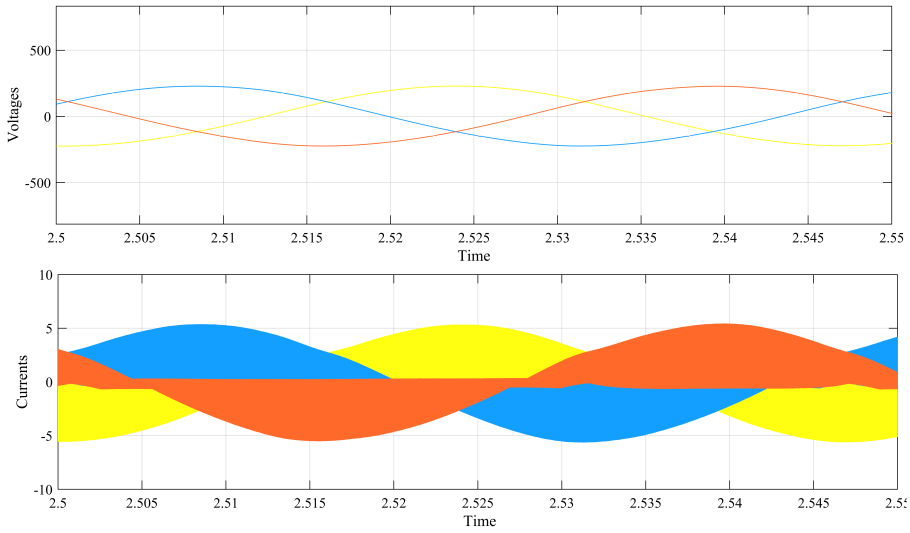

Figure 4.8: Input current and voltage waveform

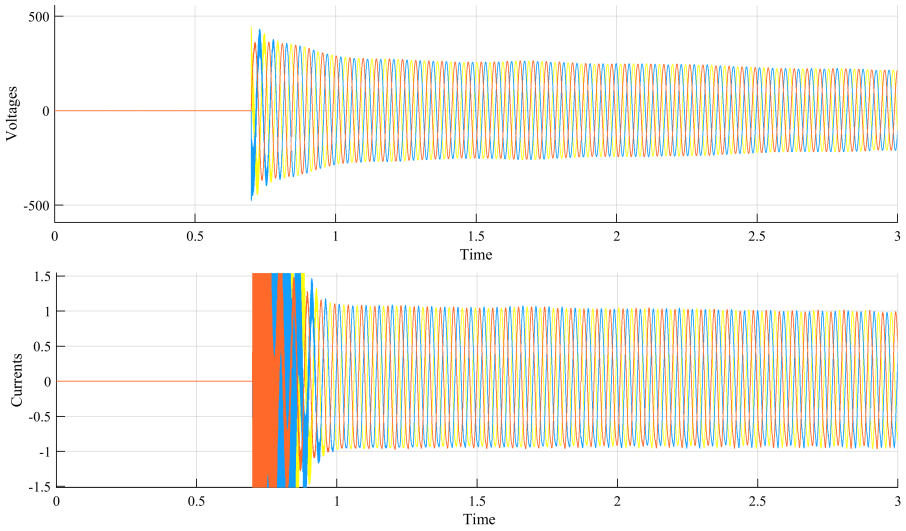

Figure 4.9: Voltage and current waveform from source

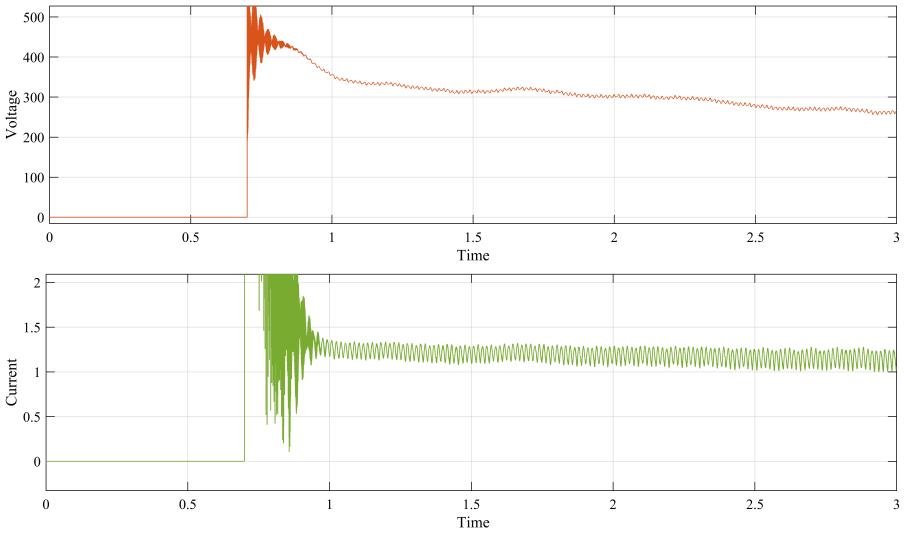

Figure 4.10: Calculated voltage and current maxima

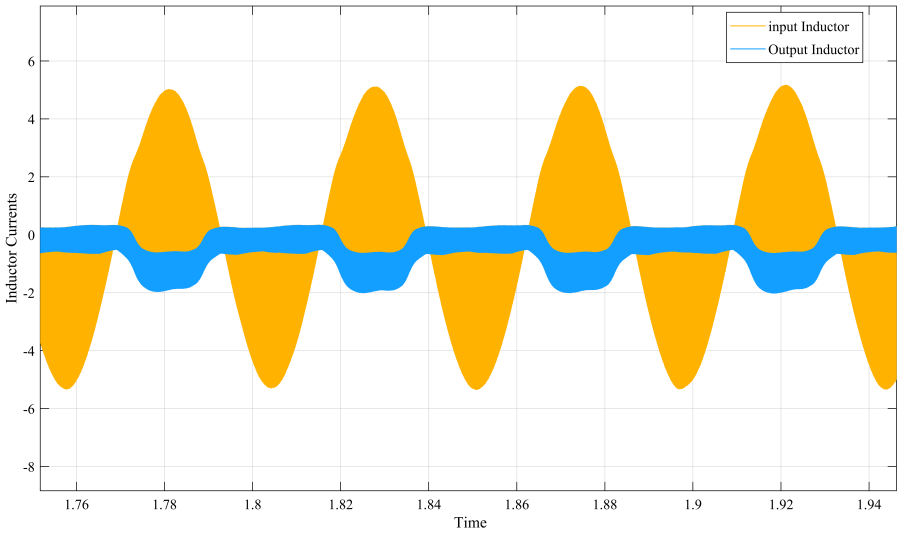

Figure 4.11: Current waveform of input and output inductors

current is in CICM around the maxima and in DICM around zero crossings of the input voltage. This drawback is compensated by the 120° phase-shifted output currents in the three output inductors, which results in lower output voltage ripple.

Figure 4.12a shows the variation of the duty as per the methodology shown in Figure 4.7; the generator is connected to the converter at 0.7 sec. In the simulation, a system consisting of a DC motor-based wind emulator and SEIG is considered, which increases the overall settling time. The MPPT technique is found to be robust enough to respond satisfactorily. The variation of the output voltage with duty variation is shown in figure 4.12b.

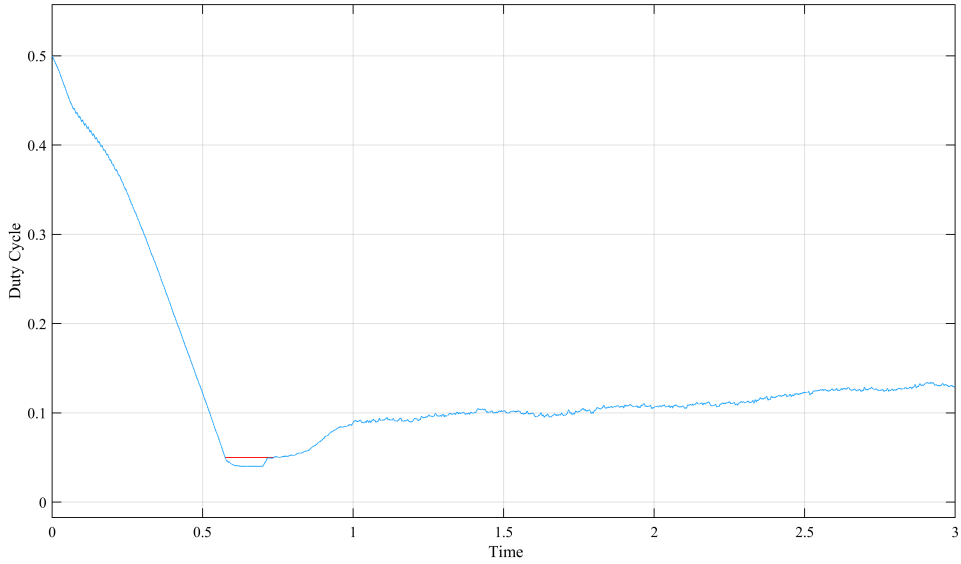

(a) Duty variation for MPPT

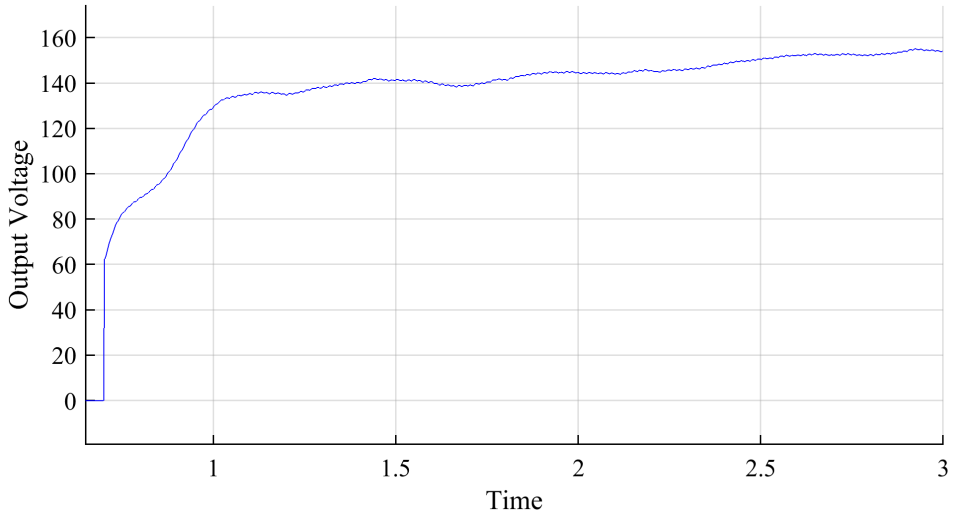

(b) Output voltage of the converter

Figure 4.12: MPPT characteristics

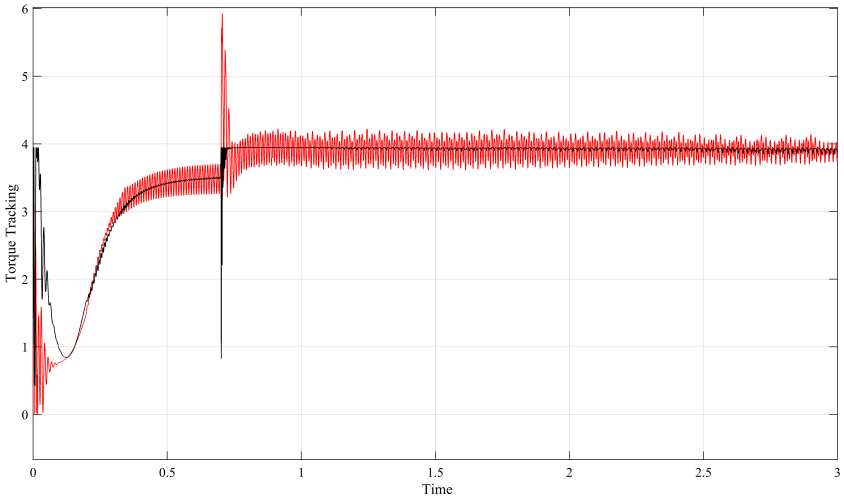

(a) Tracking of the generated reference torque

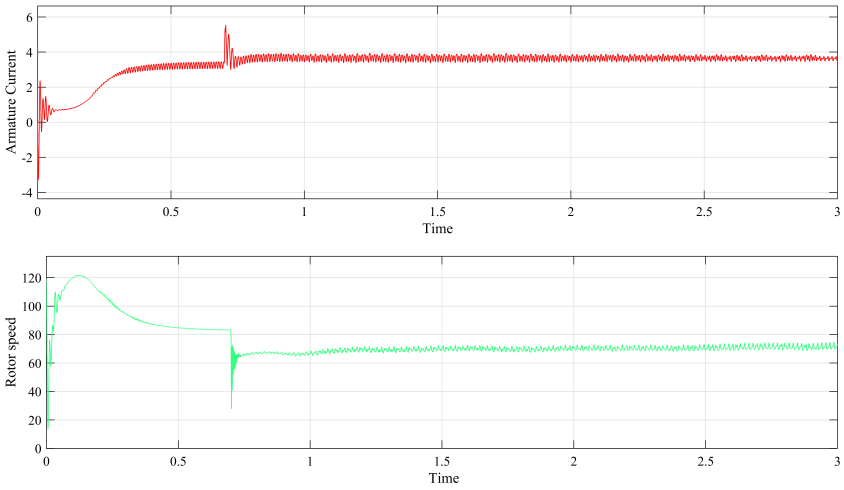

(b) Armature current(A) and speed(rad/s) of the turbine emulator

Figure 4.13: Wind turbine emulator response

Figure 4.13a shows the tracking of the reference torque by the DC motor. The higher value of K_i ensures stable operation of the controller with a high ripple current drawn by the DC-motor.

In Figure 4.13b the simulated current and speed waveform of the DC-motor is shown. The sudden decrease in the speed is due to the loading of the SEIG at 0.7 s. After loading the generator, the MPPT technique controls the converter duty, and the emulation logic controls the current from the buck converter in order to follow the intended torque-speed characteristic of the wind turbine.

4.5 Hardware Results and Discussion

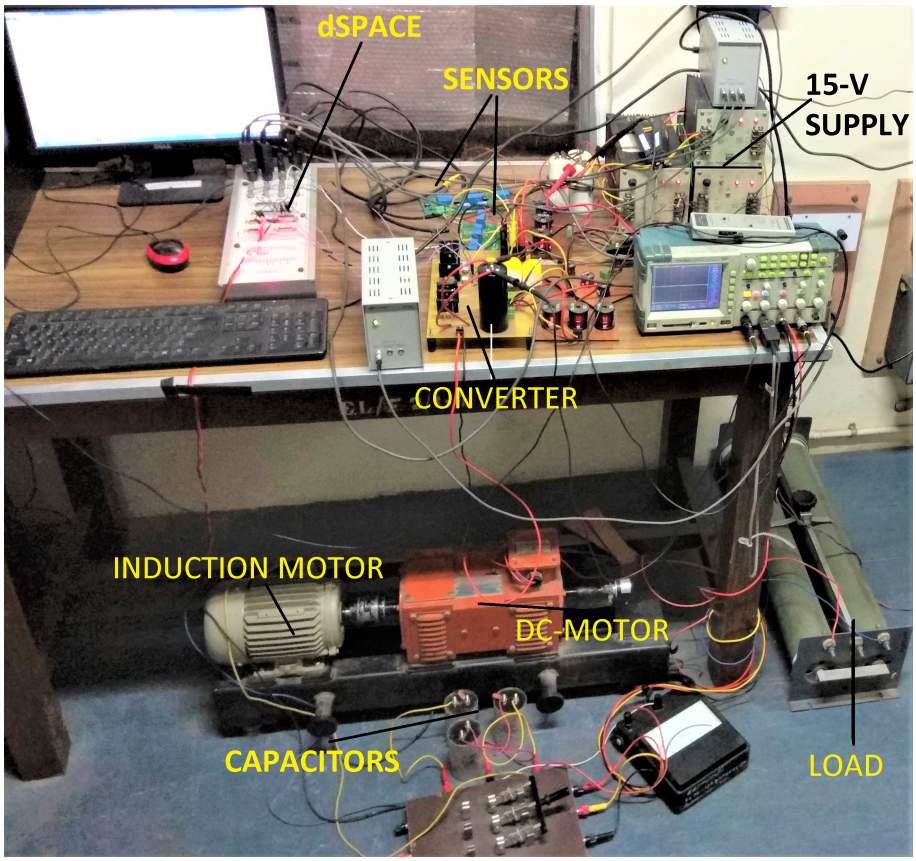

Figure 4.14: Experimental setup

DSpace-CP1104 is used to develop the hardware prototype for this work. NTHL040N65S3F MOSFET transistor is used for switching with FOD3184 optocoupler. The details of the components used are given in Table 4.4. The laboratory setup for the WECS development is shown in Figure 4.14

Figure 4.15 shows the input current waveforms of the converter under loaded condition. The input inductor currents in phases having negative voltages are also in the negative direction as the input inductors are working in DICM. An instance of currents waveform is shown in Figure 4.16, where phase A has a positive voltage and thus has positive current (channel-3), while the other two phases carry negative currents(channel-1&2), and output voltage on channel 4 is constant.

The PFC in the proposed converter is shown in the Figure 4.8 & 4.17, the per phase voltages and currents are found to be in phase. The high frequency switching of the input current can be easily filtered by a small LC low-pass filter.

Table 4.4: COMPONENT SPECIFICATION

COMPONENT	ATTRIBUTES	Nos
MOSFET	650 V, 65 A	3
DIODE	ULTRAFAST, 1KV, 65 A	3
OPTOCOUPLER	FOD3184, 3 A	3
DC FILM CAPACITOR	1 μF 1.2 KV	3
ELECTROLYTIC CAPACITOR	1000 μF, 600 V	1
INDUCTOR	47 μH	3
INDUCTOR	560 μ H	3

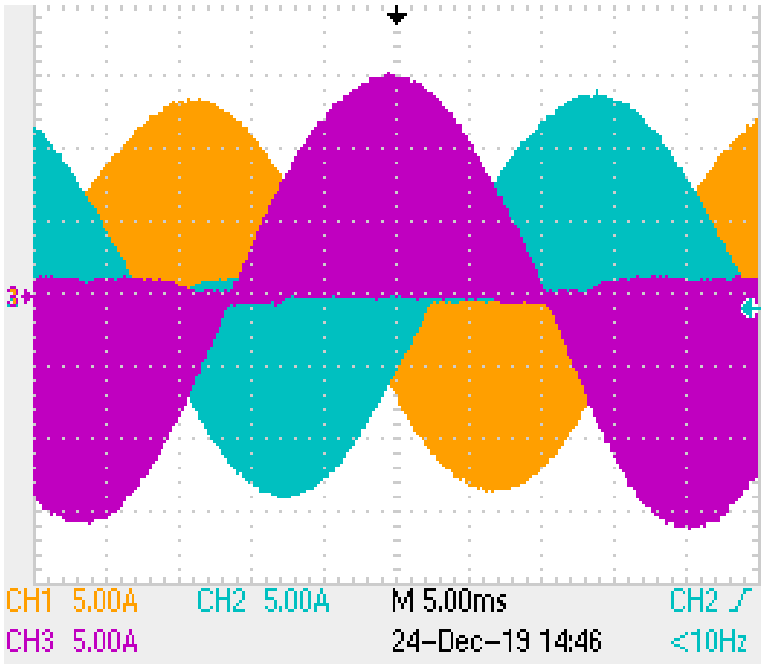

Figure 4.15: Input inductor current waveform (I_{peak}=15 A).
Current in R phase(channel-3 at 5 A/div), Y phase(channel-1 at 5 A/div), B phase(channel-2 at 5 A/div)

Figure 4.18 shows the variation of the generated voltage, current drawn from the SEIG (channels 1 & 2), and the output voltage on channel 4. The transients in voltage and current on the connection of the converter to the generator are shown in Figure 4.19. It can be observed that the transient phase passes in under 25 ms.

In Figure 4.20, the voltage build-up of the SEIG is shown. A change in the generated voltage (channel-1) is observed on connecting the converter to the generator, which is

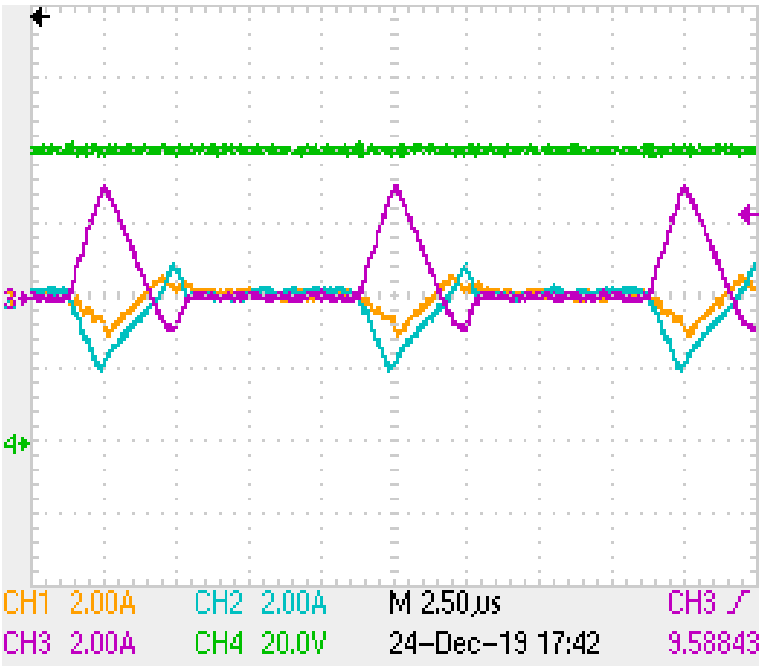

Figure 4.16: Current waveforms at 10 percent duty, current in R phase (channel-3 at 2A/div), Y phase (channel-1 at 2 A/div), B phase (channel-2 at 2A/div) and output voltage on channel 4 at 20 V/div

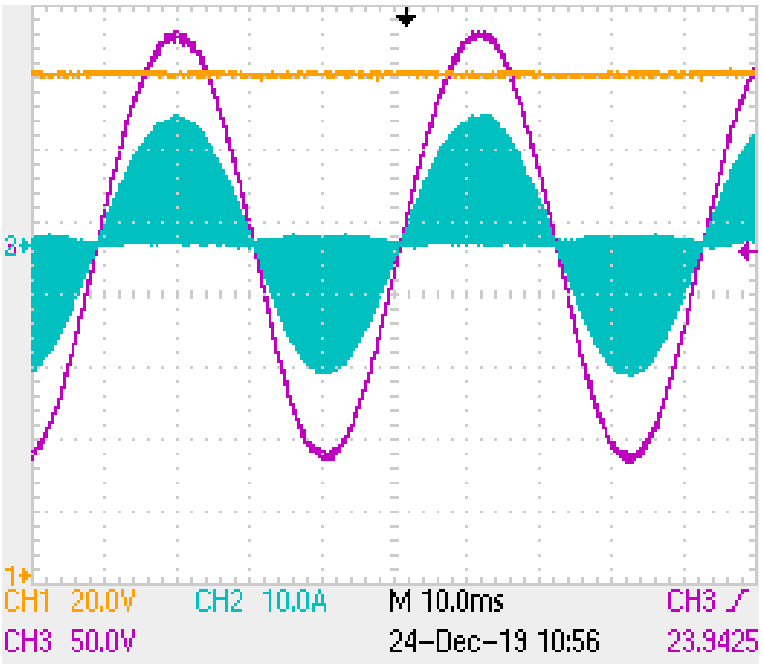

Figure 4.17: Voltage of R phase (channel-3 at 50 V/div) and input current (channel-2 10 A/div) and output voltage of the converter (channel-1 at 20 V/div)

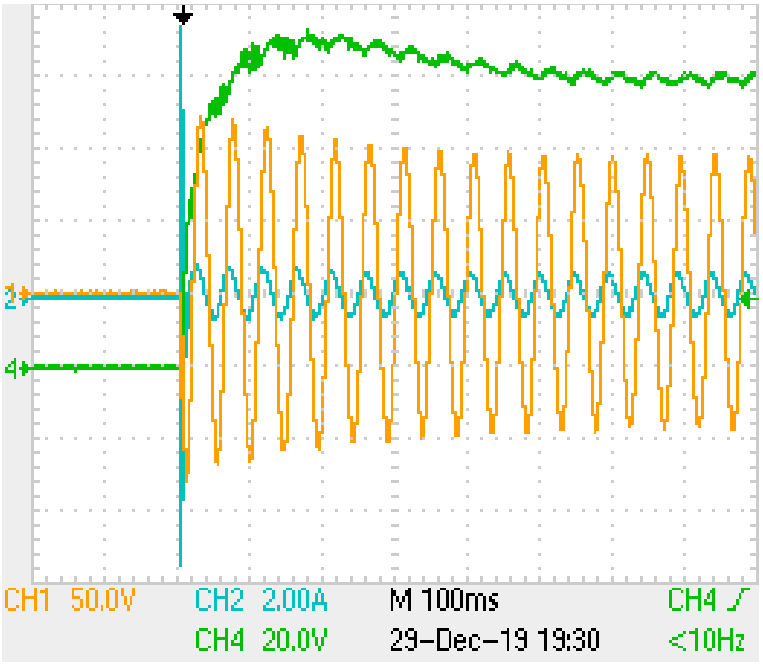

Figure 4.18: Generator voltage (channel-1 at 50 V/div) and current (channel-2 at 2 A/div) with output voltage of converter (channel-4 at 20 V/div)

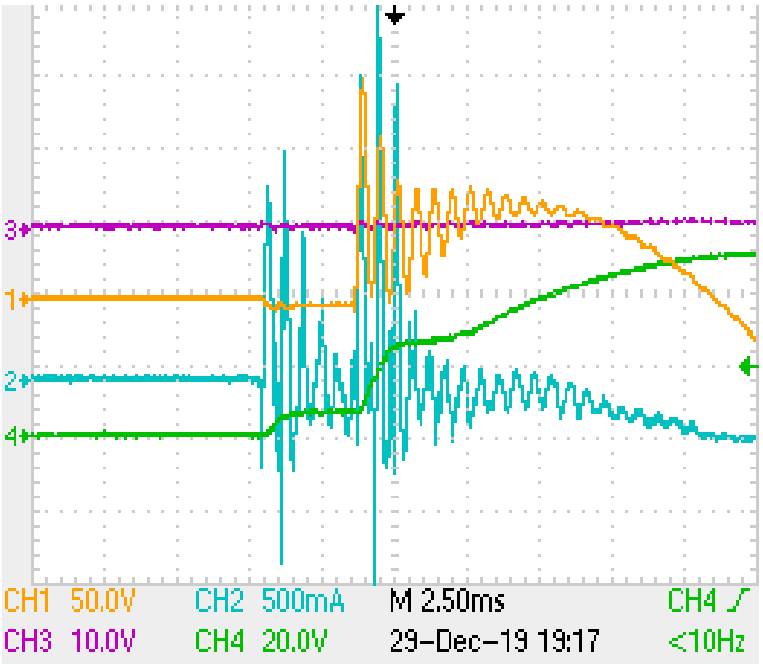

Figure 4.19: Transient filter voltage (channel-1 at 50 V/div) and current (channel-2 at 500 mA/div) waveforms and output voltage(channel-4 at 20 V/div)

marked by an increase in the output voltage (channel-4) and generator current(channel-2). The speed is measured by the encoder and then is converted to an analog signal using a DAC ($1V/400RPM$), which is shown on channel 3.

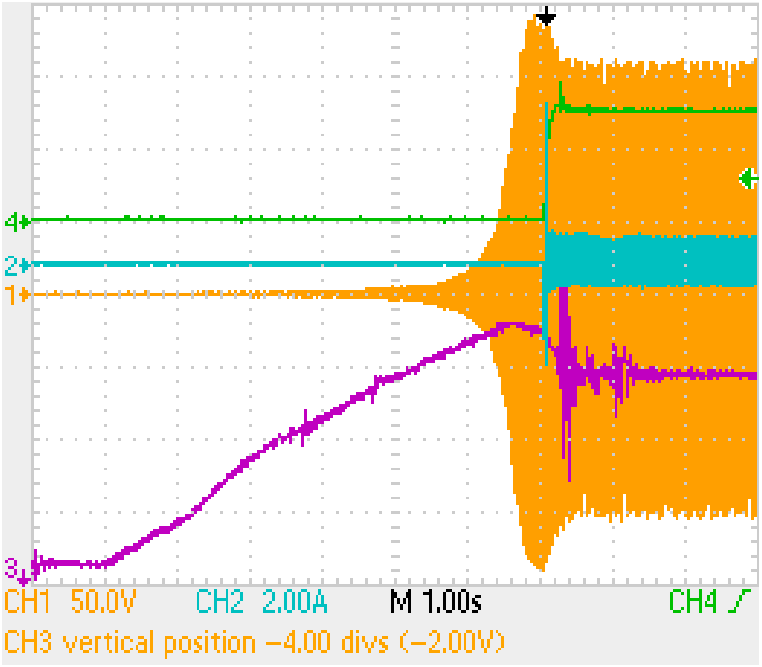

Figure 4.20: SEIG voltage buildup (channel-1 at 50 V/div), generator current(channel-2 at 2 A/div), speed of SEIG(channel-3 at 200 RPM/div) and output voltage(channel-4 at 100 V/div)

4.6 Summary

A new Three-phase bridgeless ćuk converter is proposed, analyzed, and validated in this chapter. The proposed single-stage converter is found suitable for three-phase generators as it eliminates front-end DBR. The DICM operation of the input inductor ensures lesser switching stress and inherent PFC. The wide range of output voltage control of the ćuk converter leads to better MPPT technique implementation. An MPPT control based on three-phase voltages and currents is also reported, which eliminates the need for an intermediate DC stage. The satisfactory results obtained from the SEIG-based wind generation system are indicative of the suitability of the converter's application in standalone WECS.

The implementation of the developed bridgeless ĉuk converter with a PMSG fed

WECS is dealt with in the next chapter. The drawbacks of low voltage constant and failure of generation at low wind speed is mitigated by using PMSG based generation system.